ISSN 1392–1320 MATERIALS SCIENCE (MEDŽIAGOTYRA). Vol. 13, No. 3. 2007

Investigation of Silver Polymer Nanocomposites

Igoris PROSYČEVAS[1], Judita PUIŠO[1,2*], Asta GUOBIENĖ[1,3], Sigitas TAMULEVIČIUS[1,2], Ramūnas NAUJOKAITIS[2]

[1]*Institute of Physical Electronics of Kaunas University of Technology, Savanorių 271, LT-50131, Kaunas, Lithuania*
[2]*Department of Physics, Kaunas University of Technology, Studentu 50, LT-51368 Kaunas, Lithuania*
[3]*International Studies Center of Kaunas University of Technology, Mickevičiaus 37, LT-44244 Kaunas, Lithuania*

Received 29 May 2007; accepted 01 August 2007

The aim of this work is to produce and investigate silver polymer nanocomposites formed by electron beam evaporation on PMMA-PET structure. It is demonstrated that the surface plasmon resonance (SPR) absorption peak of nanostructured silver is near 425 nm and shifts to the longer waves (up to 600 nm) and corresponding band broadening with increase of silver film thickness. The different ultrathin silver-polymer nanocomposites color filters as a result of plasmon resonance shifting in the UV-VIS wavelength region were produced. The developed method provided a simple and practical solution to create silver nanostructures in polymer matrix.

Keywords: polymethylmethacrylate (PMMA), polyethylene terephthalate (PET), silver, nanocomposites, plasmonic optic, AFM.

INTRODUCTION

Nano- and thin-film technologies based on novel systems associating metals particles to polymer matrix open a broad range of new applications in as optical fibers, sub-wavelength waveguides, nonlinear optical switches [1], superlens [2], magnetooptic data storages, directional connectors, electronics as nanowires [3] for biomedical materials nanoparticle barcode labels [4 – 5], sensitive materials for DNA screening [6] biosensors [7], as well as bio-films with anti- microbial effects of Ag [8] materials. The properties of composite materials can be tailored by changing particle size, size distribution or shape of particles [9]. The key problems in this area involve synthesis, functionalization of the nanoparticles and dispersion in a polymer matrix. Among various polymers, PMMA is highly transparent plastic with good mechanical strength and is used variously from commodities to industrial applications. Accordingly, the PMMA is a candidate substrate for optical and medical applications [10 – 11] as bone cement, dialyser, scaffolds for tissue engineering and potential candidate to waveguide production [12]. Poly(ethylene terephthalate) (PET) is used in cardiovascular implants such as artificial heart valve sewing rings and artificial blood vessels because of its excellent mechanical properties and moderate biocompatibility.

This paper presents the research on silver nanostructures in PMMA-PET structure formation by electron beam evaporation.

EXPERIMENTAL

Synthesis of the PMMA-PET structure

Poly-methylmethacrylate (PMMA – "Plexiglas" or "Perspex") with molecular weight equal to 110000 (a.m.u.) was dissolved in chloroforme (5 wt.% polymer in solvent) and dip coated on the plasma processed (RF = 13.56 MHz, P = 0.3 W/cm^2, t = 60 s) PET substrate. As a substrate a PET of Sigma Aldrich, with a thickness of 25 μm was used. PET substrates were dipped in the dissolved polymer for about 10 – 20 seconds. The dip-out time was 10 minutes. The samples were dried out in a chamber at constant moisture (humidity 60 %, atmospheric pressure) for 1 hour.

Formation of the Ag-PMMA-PET structure

PMMA-PET structures were metallized with silver Ag (purity 99.9 %, Sigma Aldrich, UK) thickness of 1, 5, 10, 15 and 20 nm by electron beam evaporation at room temperature (residual gas pressure 10^{-5} Pa, T = 293 K average deposition rate ~0.7 nm/s). Film thickness during deposition was monitored with a quartz balance technique. The temperature of the substrates during deposition was controlled with the accuracy of ±0.5 °C. The films were prepared at room temperature.

Characterization of the Ag-PMMA-PET structure

The silver amount in the polymer structure was defined with a X-ray fluorescence spectrometer VRA-20 operating at 350 kV and 26 mA, at registration time 30 s, and radius of the analyzed surface – 10 mm.

The X-ray diffraction measurements for the films were recorded at room temperature in a DRON-3.0 difractometer using Ni-filtered CuK_α radiation operating at 30 kV and 30 mA in a step scan mode with a step size of 0.02° for 2θ and registration time of 20 s per step. XRD analysis of Ag films on PET was performed to define values of interplanar distance d_{111}, lattice constant as well as grain size and microstrain. Winfit! 1.2 software was used in these calculations. T. Walker, Single line method for analysis of X-ray diffraction line broadening using a Pseudo-Voigt profile function software was employed.

The optical absorbance of the films was measured by the spectrometer UV-VIS-26 in the 300 nm – 800 nm

*Corresponding author. Tel.: +370-37-314423; fax: +370-37-314423.
E-mail address: *judita.puiso@fei.lt* (J. Puišo)

wavelength ranges (accuracy of the absorbance measurements 0.2 %). Gaussian approximation of the absorbsion peak was used respectively. The theoretical calculation of extinction-cross-section versus wavelength and silver particle size were done with MiePLOT software using silver particle dispersed in PMMA matrix. Theoretical predictions of the SPR peak were made using Mie calculations, performed on Mieplot. In the calculations, refractive indexes for surrounding media (PMMA) complex refractive indexes of bulk silver [13] were used for NPs, silver particles were assembled to be with normal distribution (standard deviation 20 % and 40 %, $N = 50$). According to [14] optical spectra of spherical nanoparticles embedded in various dielectric media were simulated in terms of the Mie electromagnetic theory, which allows one to estimate the extinction cross section σ_{ext} and elastic scattering σ_{sca} for a wave incident on a part. Mie and Steubing [9] reported that for gold particles <20 nm, absorption dominates the optical properties and for gold particles >20 nm scattering dominates the optical properties. For samples with electromagnetically non-interacting nanoparticles, it is possible to put experimental absorbance $\sim\sigma_{sca}$. Therefore, experimental absorbance spectra can be compared with model spectral dependences that are expressed through σ_{ext} from the Mie theory.

Electrical properties of the films were determined by measuring the sheet resistance with original four-point probe equipment.

Atomic force microscope NANOTOP-206 operating in a contact mode (cantilever force constant 0.9 N/m) was used to investigate morphology of the surface. Image processing and analysis of scanning probe microscopy data was performed using a Windows-based program "Surface View 2.0". Statistical evaluation of the surface morphology was performed for the scanning area 13 μm × 13 μm.

RESULTS AND DISCUSSION

XRF analysis

Dependence of amount of silver in PMMA-PET as versus thin film thickness that was registered during deposition is shown in Fig. 1.

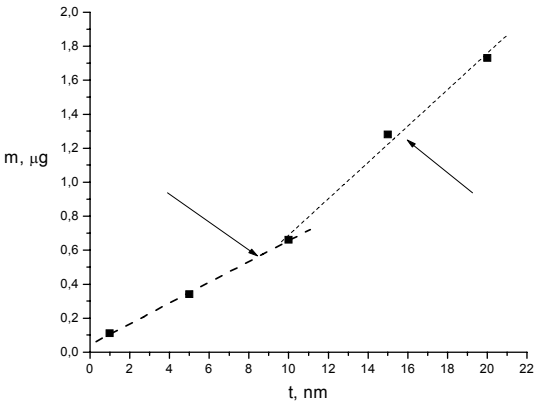

Fig. 1. Dependence of amount of silver in PMMA-PET versus thin layer thickness

The critical point of silver atoms adsorption on polymer PMMA-PET is observed at 10 nm of silver thickness on PMMA-PET. Our results suggest that discontinuous (islands) silver layer was formed at the initial growth stage of silver layer on polymer substrate PMMA-PET substrate (below 10 nm), later the formation of continuous silver film was observed with increasing thin film thickness.

XRD analysis results

The XRD pattern of 1, 5, 10, 15 and 20 nm Ag on PMMA-PET are presented in Fig. 2. XRD peaks of Ag films on PMMA-PET substrates corresponding to (111), (200) planes were observed. The peaks of 1 nm and 5 nm Ag films were very weak, but the relative intensity of (111) peak is significantly higher than that for Ag powder diffraction [15]. Preferred orientation of some Ag grains starting at very early growth stages is explained from a viewpoint of thermodynamics, i. e. the preferred orientations of thin films are known to be the perpendicular directions to the planes of lowest surface energy [16], which correspond to the most densely packed planes. For silver it is (111) plane. Initial orientations of nuclei are governed by the adsorption energy of adatoms to substrate and bonding energy between adatoms. In general, island type growth mode (Volmer-Weber growth mode) is classified into two types according to wettability of substrates. Wetting mode nuclei have smaller contact angles and preferential orientations. On the contrary, nuclei of non-wetting mode usually orient randomly. Metals of low reactivity as silver do not wet untreated polymer surfaces and exhibit a Volmer-Weber growth mode, i. e. they form clusters on the surface, which finally coalesce at high metal coverage [17]. Our results suggest that Ag films grow in wetting mode (or the secondary nucleation take a place during film growth [18]).

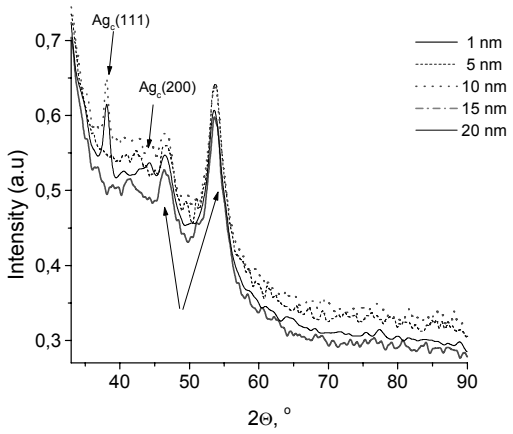

Fig. 2. XRD pattern of Ag films on PMMA-PET substrate of different thickness

The crystallite size and microstrain of the Ag film calculated according to [9] are presented in Table 1. The crystallite size for the Ag films (Table 1) increased from 28.52 nm to 32.91 nm with increment of Ag film thickness from 10 nm to 20 nm. According to the X-ray diffraction studies of 15 nm Ag films onto a glass or quartz slide consists of isolated metal islands of approximately 10 nm – 60 nm in diameter on PET [18 – 19]. At low thickness (up to 10 nm) the crystallite size is equal to the film thickness.

Above a thickness of 10 nm the crystallite size is still proportional to the film thickness, but the crystallite growth is slower than the increment in the film thickness [18]. The microstrain increased with the increasing of Ag thickness on the PMMA-PET surface. For comparison the grain size of 20 nm Ag film on PET (with the same parameters of deposition) was 11.6 nm and microstrain was 0.87 %. Our results suggest crack formation in continuous films and formation of large grain size discontinuous silver films on PMMA-PET substrate due to thermal stress (difference of coefficients of thermal expansion of Ag (8.6×10^{-6} K^{-1}) and PMMA ($70 - 77 \times \times 10^{-6}$ K^{-1}) and PET ($20 - 80 \times 10^{-6}$ K^{-1})).

Table 1. The crystallite size and microstrain of Ag films on PMMA-PET and Ag films on PET

Thickness, nm	D (crystallite/domain size), nm	ε (strain), %
10	28.52	0.73
15	15.32	0.85
20	32.91	1.13
20 nm on PET	11.6	0.87

Electrical properties in dependence on the film thickness

The Ag film conductivity varied from $5.21 \cdot 10^4$ Ω^{-1}cm^{-1} to $9.43 \cdot 10^3$ Ω^{-1}cm^{-1}. The conductivity decreased with Ag thin layer thickness. Our results suggest that a certain minimum film thickness needed to state metallic conductivity is 15 nm. According to [19 – 20] in the initial stages of the film growth only isolated islands exist on the substrate due to the Volmer-Weber growth mode of Ag on PET. At the percolation threshold (3.2 nm – 9.2 nm), where a percolating cluster is in the order of magnitude of the whole substrate surface is formed, the onset of metallic conductivity should be found. The reason for the increase of the conductivity with film thickness above point of transition from island to a closed film (11.6 nm – 18.2 nm of Ag film thickness) is caused by the reduced influence of the scattering of electrons at the outer surface of the film and by grain growth [20]. In our case conductivity values were lower than the ones of the bulk silver indicating possible silver atoms diffusion to the polymer matrix (Conductivity values were much higher than typical polymers conductivity values ~$5 \cdot 10^{-15}$ Ω^{-1}cm^{-1}). According to [20] when the volume fraction of nanosized silver in polyvinyl acetate emulsion is high as 0.848 (or 98.2 wt %) its conductivity becomes $5.18 \cdot 10^3$ Ω^{-1}cm^{-1}. When the volume fraction of nano-sized silver decreases to 0.335 (corresponding weight percent ~83 %), conductivity becomes $1.25 \cdot 10^{-3}$ Ω^{-1}cm^{-1} which might be close to the threshold value for this composites.

AFM analysis

Fig. 3 and Table 2 presents the AFM images and statistical analysis of morphology of evaporated and annealed Ag films on PMMA-PET structure. The difference in microstucture and particle shape of discontinuous Ag samples are clearly seen. The average roughness (Fig. 4) of PET before and after plasma treatment was 1.05 nm and 3.74 nm. After PMMA layer formation (133.28 nm), the PET surface with fairly high peaks was filed and PMMA structure was such as porous surfaces with fairly deep valleys in the smoother plateau (surface skewness varied from 0.80 nm to –0.74 nm). We suggest that the roughness variations are related to the three steps of silver film growth:

I) nucleation and island formation at the initial stages of the film growth. The roughness of PMMA surface after deposition of 1 nm and 5 nm silver increases up to 644.09 nm, but the variation of skewness indicated, that the PMMA surface with silver become smoother (between the thickness values 1 nm – 5 nm, the average roughness increases);

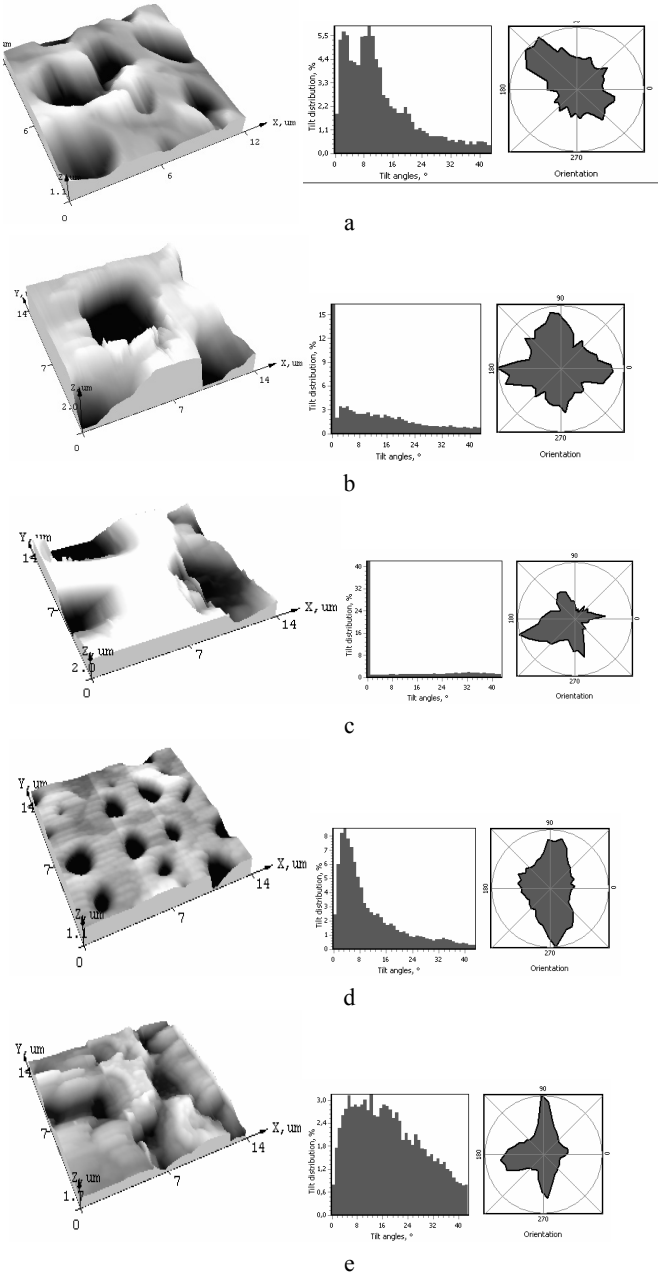

Fig. 3. Ag layer of different thickness on PMMA-PET substrate: a – PMMA-PET structure (without Ag); b – 1 nm, c – 5 nm; d – 10 nm and e – 20 nm

Table 2. Morphology and grain size of Ag films on PMMA-PET

Para meter	PMMA-PET	1 nm (Ag)	5 nm (Ag)	10 nm (Ag)	15 nm (Ag)	20 nm (Ag)
R_a	133.2	587.3	644.0	95.8	228.1	232.4
R_q	170.1	675.5	726.6	145.1	293.5	290.9
R_{sk}	–0.74	–0.75	–0.64	–2.42	–0.05	–0.40

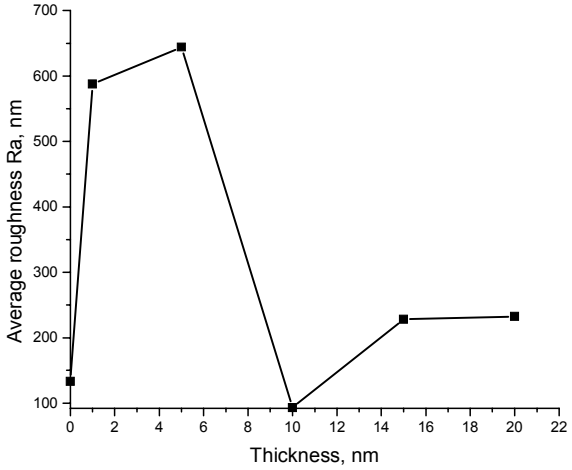

Fig. 4. Dependence of the roughness of Ag films on thin film thickness

II) decrease of the average roughness and increasing negative skewness values with the increasing film thickness (between the thickness values 5 nm – 10 nm) could be related to the lateral island growth on the surface of Ag-PMMA-PET structure, also to the filling by silver atoms the deep valley of polymer matrix;

III) continuous film growth (from 15 nm of silver thin film thickness).

Our results are in good agreement with [15] proposed of sputter silver thin film growth on PET substrate model. On the other hand one should account dynamics of motion of PMMA macromolecules in high vacuum. According to [15] filler particles with radius smaller than the bulk radius of gyration of the polymer chain act as effective entanglement sites. Experimentally reduction in chain mobility is observed with filler radius and the dramatic loss of mobility in nanocomposites is comparable with the filler size.

Optical properties of Ag layers on PMMA-PET

The absorption spectra of silver on PMMA-PET substrate are shown in Fig. 5.

For the lowest thickness, the surface plasmon resonance (SPR) absorption peak is near to 425 nm and shifts to the longer waves (up to 600 nm) with thickness, with the band broadening significantly. The peak of this band is not high, although it is related to the SPR effect in the silver nanoparticles. It is in good agreement with [17] results of silver implantion to PMMA substrate. According to [17] the absorption peak of 10 nm – 20 nm PMMA grains is observed at 602 nm – 617 nm regions of absorption spectra. The spherical particles are observed at lower thickness. Extinction spectra for Ag nanoparticles (1 nm – 5 nm Ag thickness) embedded in a polymer matrix were computed and compared with the experimental data shown in Fig 6.

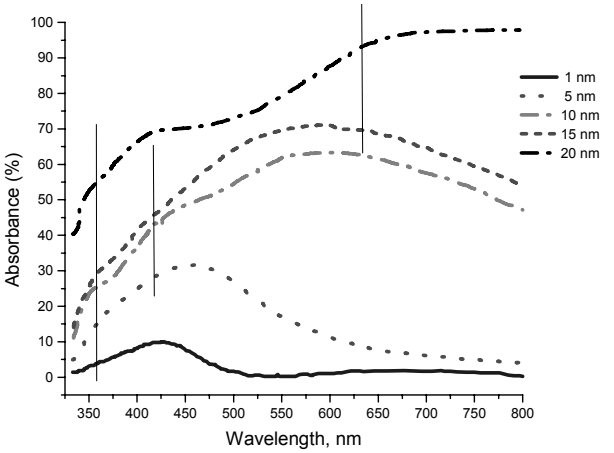

Fig. 5. Absorbance spectra of Ag-PMMA-PET structure

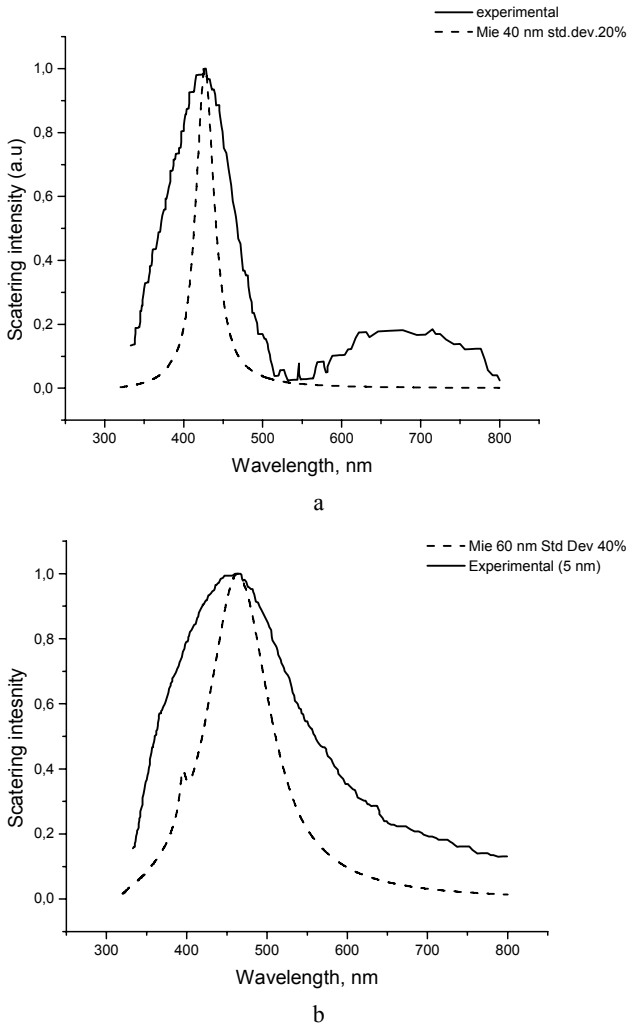

Fig. 6. Spectra of Ag spherical particles in PMMA matrix at different thickness of Ag film: a – 1 nm and b – 5 nm

According to [9] we observed "blue" particles (scattering light between 400 nm to 480 nm) that are roughly spherical (diameters 40 nm – 90 nm) at the low thickness of silver layer (1 nm), "green" particles (500 nm – 550 nm) – typically hexagonal (longest dimension – 60 nm – 105 nm), and "red" particles (600 nm – 700 nm)

with a triangular cross section (longest dimension – 55 nm – 120 nm) at the higher thickness. According to [3, 6, 22] we observed the non-spherical particles (nanorods, nanowires or nanodisk) with transverse and longitudinal SPR peaks of rod-shape silver nanostructures at 352 nm and 630 nm. The peak at 414 nm indicated the formation of silver nanoparticles with a diameter ~30 nm. (Mie calculation results).

CONCLUSION

The properties of silver – polymer nanocomposites vary with the silver layer thickness. XRD, conductivity and morphology measurements suggest that the silver layer growth on PMMA-PET could be described by the wetting Volmer-Weber thin film growth model. The silver discontinuous (island) layer with preferred (111) orientation is formed at the initial growth stage (1 nm – 10 nm). The formation of continuous films is observed with increasing the Ag layer thickness. The crystallite size for the Ag films increased from 28.52 nm to 32.91 nm with increment of Ag film thickness. The microstrain inceased with increament of the Ag layer thickness. The metal-polymer conductivity was $5.21 \cdot 10^4\ \Omega^{-1}cm^{-1}$to $9.43 \cdot 10^3\ \Omega^{-1}cm^{-1}$. The optical spectra of silver – polymer PMMA-PET nanocomposites revealed the presence of the silver nanoparticle surface plasmon. The nanocomposites produced by variation of silver layer thickness were shown shifting the plasmon resonance wavelength in the UV-VIS region and look promising in producing of ultrathin colour filters.

Acknowledgements

The Lithuanian Science and Study Foundation has supported this work.

REFERENCES

1. **Kampf, G., Dietze, B, Große-Siestrup, C., Wendt, C., Martiny, H.** Microbicidal Activity of a New Silver-Containing Polymer, SPI-ARGENT II *Antimicrobial Agents And Chemotherapy* 42 1998: pp. 2440 – 2442.
2. **Fang, N., Lee, H., Sun, C., Zhang, X.** Sub-Diffraction-limited Optical Imaging with Silver Superlens *Science* 308 2005: pp. 534 – 537.
3. **Sun, Y., Gates, B., Mayers, B., Xia, Y.** Crystalline Silver Nanowires by Soft Solution Processing *Nano Letters* 2 2002: pp. 165 – 168.
4. **Nicewarner-Pena, S. R., Griffith Freemean, R., Reiss, B. D., He, L., Pena, D. J., Walton, I. D., Cromer, R., Keating, C. D., Natan, M. J.** Submicrometer Metallic Barcode *Science* 294 2001: pp. 137 – 141.
5. **Mock, J. J., Oldenburg, S. J., Smith, D. R., Schultz, D. A., Schultz, S.** Composite Plasmon Resonant Nanowires *Nano Letters* 5 2002: pp. 465 – 469.
6. **Mailard, M., Huang, O., Brus, L.** Silver Nanodisk Growth by Surface Plasmon Enhanced Protoreduction of Adsorbed [Ag+] *Nano Letters* 3 2003: pp. 1611 – 1615.
7. **Haes, A. J., Stuart, D. A, Nie, S., Van Dyyene, R. P.** Using Solution-Phase Nanoparticles, Surface – Confined Nano-particle Arrays and Single Nanoparticles as Biological Sensing Platforms *Journal of Flourescence* 14 2004: pp. 355 – 367.
8. **Mock, J. J., Barbic, M., Smith, D. R., Schultz, D. A., Schultz, S.** Shape Effects in Plasmon Resonance of Individual Colloidal Silver Nanoparticles *Journal of Chemical Physics* 116 2002: pp. 6755 – 6759.
9. **Boldyryeva, H., Umeda, N., Plaskin, O. A., Takeda, Y., Kishimoto, N.** High-fluence Implantation of Negative Metal Ions Into Polymers Surface Modification and Nanoparticle Formation *Surf. Coat. Techn*. 196 2005: pp. 373 – 377.
10. **Hong, W., Woo, H-J., Choi, H-W., Kim, Y-S, Kim, G-D.** Optical Property Modification of PMMA by Ion-beam Implantation *Appl. Surd. Sci*. 169 – 170 2001: pp. 428 – 432.
11. **Johnson P. B. and Christy R. W.**, Optical Constants of Noble Metals, *Physical Review* B, Volume 16, (1972), pp. 4370 – 4379,
12. **Xia, Y., Halas, X, J.** Shape-Controlled Synthesis and Surface Plasmon Properties of Metallic Nanostructures *MRS Bulletin* 30 2005: pp. 338 – 348.
13. **Thran, Kiene, M., Zaporojchenko, V., Faupel, F.** Condensation Coefficients of Ag on Polymers *Physical Review Letters* 82 1999: pp. 1903 – 1906.
14. **Picu, R. V., Ozmusul, M. S.** Enhanced Struture at the Interface Between the Polymer Matrix and Spherical Nanoparticles in Polymer Based Nanocomposites www.asc5004.com.
15. **Pang, I., Shen, Y., Tetz, K., Fainman, Y.** PMMA Quantum Dots Composites Fabricated Via Use of Pre-polymerization *Optics Express* 13 2005: p. 44 – 49.
16. **Fukuda, S., Kawamoto, S., Gotoh, Y.** Degradation of Ag and Ag-alloy Mirrors Sputtered on Poly(ethylene terephthalate) Substrates Under Visible Light Irradiation *Thin Solid Films* 442 2003: pp. 117 – 120.
17. **Biswas, A., Aktas, O. C., Kanzow, J., Saeeda, U., Strunskus, T., Zaporojtchenko, V., Faupel, F.** Polymer – Metal Optical Nanocomposites with Tunable Particle Plasmon Resonance Prepared by Vapor Phase Co-Deposition *Materials Letters* 58 2004: pp. 1530 – 1534.
18. **Charton, Fahland, M.** Growth of Ag on PET Deposited by Magnetron Sputtering *Vacuum* 68 2003: pp. 65 – 73.
19. **Xia, Y., Halas, X., J.** Shape-Controlled Synthesis and Surface Plasmon Properties of Metallic Nanostructures MRS Bulletin 30 2005: pp. 338 – 348.
20. **Picu, R. V., Ozmusul, M. S.** Enhanced Struture at the Interface Between the Polymer Matrix and Sperical Nanopartilces in Polymer Based Nanocomposites. www.asc5004.com.